Journal of Dynamic Behavior of Materials
https://doi.org/10.1007/s40870-024-00425-x

S.I.: THADHANI

High Strain Rate Hardening of Metallic Cellular Metamaterials

N. Novak[1] · **M. Vesenjak**[1] · **Z. Ren**[1]

Received: 12 December 2023 / Accepted: 6 May 2024

Abstract
Strain rate hardening caused by the changed deformation mode is a fascinating phenomenon in cellular metamaterials where the material's stiffness and energy absorption capabilities increase as the strain rate increases. This unique behaviour is attributed to a combination of micro-inertia effects, base material's strain rate hardening and inertia effects. At high strain rates, the metamaterial's inertia influences its deformation response, which changes to shock mode. This work briefly presents the geometry and fabrication of different metallic metamaterials. Then, it evaluates their mechanical response at different strain rates, ranging from quasi-static to intermediate dynamic and shock, determined by experimental and computational investigation. The three deformation modes can be separated into two critical loading velocities, unique for each metamaterial, which are also presented and compared in this work for various metamaterials. The investigations show that the deformation mode change in metallic metamaterials depends on their porosity. The critical velocities separating the deformation modes decrease with increasing porosity, i.e., decreased density of the metamaterial results in reduced critical loading velocities. The shock deformation mode in cellular metamaterials is thus attainable at much lower loading velocities than in homogeneous (nonporous) materials.

Keywords Metamaterials · Cellular structures · High strain rate · Experimental testing · Computational modelling · Compression loading · Mechanical properties

Introduction

Cellular metamaterials are engineered materials with an internal cellular structure ranging from the nanoscale to the macroscale. They have attracted significant attention in the engineering and scientific community over the past decades due to their unique combination of low relative density (porosity) and exceptional multifunctional properties [1]. These properties include superior energy absorption capabilities, efficient vibration-damping characteristics, durability and excellent thermal and acoustic insulation performance. This combination makes cellular metamaterials ideal candidates for many modern lightweight engineering applications [1, 2]. The use of cellular metamaterials is presented in the literature, and readers are referred to [3–5] for further reading. Understanding and improving their design and behaviour under different loading regimes is paramount for the engineering and commercial community to increase efficiency.

In the past, most of the cellular metamaterials were examined using well-known and standardised mechanical testing methodologies such as quasi-static uniaxial compression, tension, and bending. However, technical developments in measuring equipment continue to enhance shear, dynamic, and vibroacoustic testing techniques, which can provide further insight into the deformation behaviour of cellular metamaterials [6]. The dynamic and impact behaviour of regular cellular structures has been studied to some extent using experimental and computational approaches [7]. These studies have provided valuable insights into cellular structures' energy absorption and impact resistance [8, 9]. However, little work was done on the detailed deformation mechanism analysis of cellular metamaterials with functionally graded porosity at different strain rates [10]. Additionally, the shock response of the periodic interpenetrating composites was studied recently [11], with the lack of experimental validation. Functionally graded porosity refers to the variation in porosity within the cellular structure. This variation can be

✉ N. Novak
n.novak@um.si

[1] Faculty of Mechanical Engineering, University of Maribor, Maribor, Slovenia

Published online: 20 May 2024

tailored to achieve specific mechanical properties, such as constant deceleration of impacting projectiles or constant reaction forces on structures under impact [11]. The ability to control the mechanical response of cellular metamaterials through functionally graded porosity has significant potential for applications in defence engineering and crashworthiness. For instance, these materials could be used to design protective armour that can withstand high-impact loads or to develop crashworthiness systems that can effectively absorb energy and protect occupants during collisions [10, 12]. A few successful dynamic experimental tests of auxetic cellular metamaterials have been carried out so far, and they have had minimal use for validating the FE models [13, 14]. Validation of computational models with experimental data is crucial for ensuring these models' accuracy and ability to predict the real-world behaviour of cellular metamaterials. Further research is needed to validate computational models for a broader range of cellular metamaterials and loading conditions [14]..

The strain rate sensitivity and high strain rate behaviour of new materials must be studied to be used effectively in real-world engineering applications such as crashworthiness, explosion protection, and ballistic protection. Because of its appealing lightweight and efficient energy absorption properties, the high strain rate behaviour of materials with internal cellular structures is particularly interesting. In recent years, the dynamic behaviour of contemporary cellular materials was investigated under various high-strain-rate loading circumstances, primarily utilising the Split Hopkinson Pressure Bar (SHPB) testing device. Sun et al. [15], Zhang et al. [16] and Novak et al. [17] present a detailed study of the dynamic compressive behaviour of traditional and additively built cellular materials. Some research looked at the effect of cell topology [18–20], while others made geometrical changes, such as tapering the struts of cellular materials [20]. Other research explored the effect of the production process and loading velocity up to 150 m/s on mechanical response [21]. The dynamic behaviour of open- and closed-cell aluminium foam and cell-based Voronoi lattices has been effectively and thoroughly investigated computationally [22–25]. Strut-based lattices with a negative Poisson ratio (commonly referred to as auxetic cellular structures) were also investigated under high strain rate impact, utilising SHPB [13] and the powder gun [26]. These investigations provide critical information about the micromechanics of the unit cell concerning the loading circumstances.

The research on the dynamic behaviour of cellular metamaterials is still not complete and mature since new metamaterials are emerging constantly. Still, it has already provided valuable insights into the beneficial behaviour of these materials under high strain rate loading conditions. Researching new concepts and developing new and improved metamaterials is crucial for their possible application in next-generation engineering products.

In the following, we have compiled metallic cellular metamaterials' high strain-rate testing results to investigate their strain-rate hardening and compare their energy absorption capacity.

Cellular Metamaterials

The cellular metamaterials presented in this work are categorized into groups based on their topological structure and fabrication method in the following section. A selection of these metamaterials studied at the University of Maribor, Slovenia, is shown in Fig. 1, which illustrates the development from fundamental to advanced geometries over the last two decades.

Fig. 1 Research history of cellular metamaterials: from primitive to advanced cellular geometries

Open-Cell Foams

The open-cell foam features an interconnected structure of cells, enabling it to be efficiently compressed and then naturally recover its original shape in most cases when made from polymeric materials. This property makes open-cell foam widely used in furniture for sofa cushions, foam mattresses, car seats, and acoustic and soundproofing applications.

Metallic open-cell foams are primarily produced using the investment casting method. The process begins with a porous polymer precursor, a template for the metallic foam structure. This precursor is infiltrated with a refractory slurry, a mixture of refractory materials and binders, and then dried. During combustion, the polymer precursor decomposes, while the refractory slurry hardens and forms a mould for the subsequent investment casting of the metallic matrix. The final step involves removing the moulding material, resulting in a porous metallic structure resembling the original polymer precursor [27]. The fabricated and reconstructed aluminium open-cell foam is shown in Fig. 2.

The mechanical properties of open-cell metal foams depend on several factors, including the base material's properties, the cells' morphology, and the foam's topology. The base material's influence on metal foams' properties is well-studied. Many empirically established relationships link the properties of the base material and morphology with the properties of the cellular material [1, 28]. Metals and alloys used for metal foams must have a low density (high porosity) to maintain the advantage of low relative density over conventional solid materials. For this reason, the most commonly used metals for cellular materials are aluminium, magnesium, titanium, and their alloys [29].

Many researchers have used the representative unit cell to explore the effect of cell shape on the mechanical characteristics of regular and irregular open-cell materials. The behaviour of the cell material was considered to be adequately characterised by a single, geometrically homogeneous cell. However, the cell morphology of some fabricated foams has shown numerous advantages very early [25] since the cell geometry of produced open-cell foams departs from the geometric regularity. Adding a polymer filler to the cellular structures can improve the mechanical behaviour of open-cell foam [30]. Open-cell foams can also be used to fill foam-filled tubes [31].

Closed-Cell Foams

Closed-cell foam is a type of foam with interlocking micro- and macroscopic cells that are sealed shut, preventing air or water from passing through. This foam type is stiffer than open-cell foam and water-resistant, making it highly suited to shock absorption and thermal insulation. The powder metallurgical approach [32] is used to fabricate closed-cell aluminium foams, which involves inserting an extruded, foamable precursor in a stainless steel mould in a preheated oven. The mould cavity is then filled by foaming the aluminium, silicon, and titanium hydride precursor. The moulded foam is taken from the oven and allowed to cool to room temperature. The aluminium foam is taken from the carbon steel mould and sliced to prepare the specimens for mechanical testing.

Closed-cell aluminium foams' mechanical behaviour has been comprehensively studied under free and laterally constrained compression stress conditions [35]. The same foams were also used to fill tubes (ex-situ foam-filled tubes), which improved the mechanical response. Powder metallurgical foam fabrication also enables the manufacture of closed-cell foams within tubes (in-situ foam-filled tubes) to enhance stiffness by improving bonding between the foam filler and the outer tube [36].

A particular type of closed-cell foam is Advanced pore morphology (APM) foam with a hybrid cellular structure, developed in Germany at the Fraunhofer IFAM, Bremen [37]. APM foam elements comprise sphere-like interconnected closed-cell porous structures within solid outer skin. The manufacturing procedure consists of powder compaction and rolling of AlSi7 alloy with TiH2 foaming agent to obtain expandable precursor material. The precursor material is cut into small volumes (granules), which are then expanded into spherical foam elements due to the heat reaction of the TiH2 foaming agent in a continuous belt furnace.

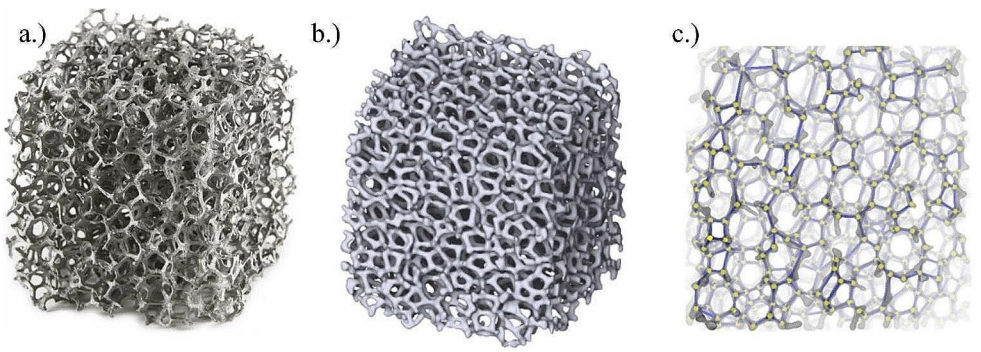

Fig. 2 Aluminium open-cell foam sample (**a**), foam surface model (**b**) and beam finite element model (**c**)

The internal structure of APM was evaluated [38, 39], and its use as a filler material for foam-filled tubes was studied [40, 41].

Closed-cell foams are a versatile material with a wide range of applications. They offer many advantages over open-cell foams, making them a good choice for applications where stiffness, water resistance, shock absorption, and thermal insulation are essential. However, they also have disadvantages, such as higher density, cost, and limited recyclability.

Predesigned Cellular Structures

Recent advances in fabrication techniques, such as additive manufacturing, have created possibilities for producing predesigned cellular structures with particular and sometimes exceptional properties. The three-dimensional auxetic cellular structures [42] and Triply Periodic Minimal Surfaces (TPMS) [43] have garnered significant attention due to their unique and advantageous characteristics.

Auxetic cellular structures, characterized by their counterintuitive property of expanding when subjected to tensile forces (negative Poisson's ratio), exhibit exceptional energy absorption capabilities and enhanced impact resistance. One notable example is the inverted tetrapod structure, which can be constructed by stacking unit cells in layers to form a three-dimensional auxetic lattice [14]. These structures have been successfully fabricated using selective electron beam melting (SEBM), demonstrating their potential for various engineering applications [44].

Chiral auxetic structures, another class of auxetic materials, exhibit a combination of auxeticity and chirality, enhancing mechanical properties and unique rotational and bending deformation mechanisms [45]. Their unit cells, inspired by the 10th eigenmode of the regular cubic unit cell, can be precisely designed and fabricated using advanced manufacturing techniques [46]. These structures are useful in lightweight applications, energy-absorbing devices, and impact-resistant structures [47].

Triply Periodical Minimal Surface (TPMS) structures, a family of complex 3D topologies, represent another exciting metamaterial frontier. These structures minimize surface area for a given boundary and can be repeated periodically in three perpendicular directions, resulting in intricate and interconnected networks [48]. TPMS have demonstrated exceptional properties in various fields, including:

- Tissue engineering: TPMS scaffolds provide a favourable environment for cell growth and differentiation, making them promising candidates for regenerative medicine applications [48].
- Structural engineering: TPMS structures exhibit enhanced stiffness, strength, and energy absorption capabilities, making them suitable for lightweight construction applications [28].
- Thermal and electrical conductivity: TPMS exhibit optimized thermal and electrical conductivity due to their unique topology, offering potential for heat sinks, electronic components, and thermal insulation applications [49].
- Fluid permeability: TPMS structures can be designed to optimize fluid permeability, making them suitable for filtration membranes, fluid flow control devices, and heat exchangers [49].

Developing advanced fabrication techniques and exploring novel material designs have opened up exciting possibilities for creating materials with exceptional properties never achievable before. Auxetic cellular structures and TPMS, with their unique characteristics and potential applications, represent promising advancements in material science that hold the potential to revolutionize various engineering fields.

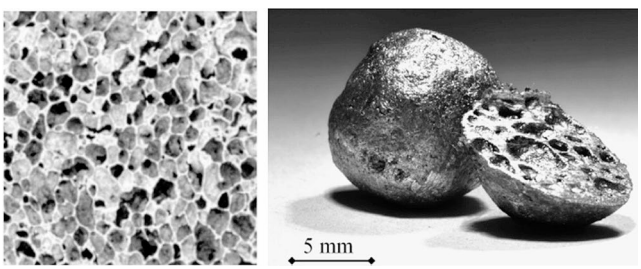

Fig. 3 Aluminium closed-cell foam sample and APM foam element [33, 34]

Methods

Fabrication of Specimens

The open-cell foam samples were manufactured by m.pore GmbH using the investment casting method described in Sect. 2.1. The base material of the foam is 99.7% pure aluminium, and the porosity of the structure is 93.9%. The foam exhibits an average pore size of 20 pores per inch (ppi). The sample was analyzed using computed tomography with X-rays (Toshiba-Aquilion 64), generating a 3D model through computational reconstruction from the set of 2D images (slices) shown in Fig. 3.

The closed-cell aluminium foam was produced using the powder metallurgical method [32] by placing extruded, foamable precursor in a cylindrical stainless steel mould in a preheated oven. After foaming, the cylindrical aluminium foam was removed from the mould made of carbon steel

and cut lengthwise to prepare the cylindrical specimens for mechanical testing.

The auxetic cellular and TPMS structures were fabricated using additive manufacturing technologies. The auxetic cellular structures analysed in this study were constructed as CAD models and produced using the selective electron beam melting method (SEBM) from the Ti-6Al-4 V and copper alloy powder at the Institute of Materials Science Technology (WTM) of the University of Erlangen-Nuremberg. The TPMS structures were fabricated using the powder bed fusion system EOS M280 from gas-atomised stainless steel 316 L powder at New York University Abu Dhabi. The strut and sheet thickness depends on various predefined parameters of the additive manufacturing machine and may differ from the original model CAD. The fabricated geometries were carefully examined using optical microscopy [11], SEM imaging [50] and CT scanning [51].

Experimental Testing

Cellular structures are generally fragile under tensile loading. They are predominantly tested under compressive loading conditions, where their unique mechanical response, characterized by elastic deformation followed by an extensive plateau stress region and densification, enables remarkable energy absorption. The typical testing methods that are used are shown in Fig. 4.

The type of test is usually determined by the deformation mode we want to achieve, namely quasi-static, transitional dynamic or shock. These deformation modes can be separated by the critical velocities for some of the metamaterials listed in Fig. 5.

Uniaxial compression tests under quasi-static loading conditions for most analyzed samples presented in this work were performed with a servo-hydraulic testing machine INSTRON 8801 with a position-controlled crosshead velocity of 0.1 mm/s (quasi-static test) and 284 mm/s (dynamic test). Adhering to the ISO 13,314: 2011 standard [52], the recorded load-displacement data was transformed into engineering stress-strain data utilizing the dimensions of the undeformed sample. The testing machine's load plates were lubricated to mitigate friction and minimize the influence of the bearing/load limit on the specimens.

At moderately increased loading velocity but still in quasi-static deformation mode, the deformation can be tracked using infrared (IR) thermography. Based on the fast-cooled middle wave (MW) infrared InSb detector camera, IR thermography detects heat dissipation during irreversible plastic deformation [53]. Capturing deformation processes is particularly advantageous due to the high frame rates of thermal image detectors, such as the employed InSb detector camera, which can reach up to 700 Hz while operating at cryogenic temperatures of -200 °C (73 K). This infrared (IR) approach facilitates observing plastification front wave propagation, plastification zones, and crack growth. Cooled medium IR wave cameras with image frequencies exceeding 100 Hz enable rapid acquisition of deformation patterns resulting from material heating during irreversible deformation. This method has demonstrated its effectiveness in visualizing deformation patterns in various cellular materials [36, 54]. However, this method is restricted to load cases at higher loading velocities, as typically used in quasi-static testing, due to heat dissipation at lower loading velocities. Visualizing the local heat dissipation of heat-conducting metals is not feasible for quasi-static loading. During tests presented in this work, IR thermographic monitoring was employed using a cooled mediumwave thermal imaging

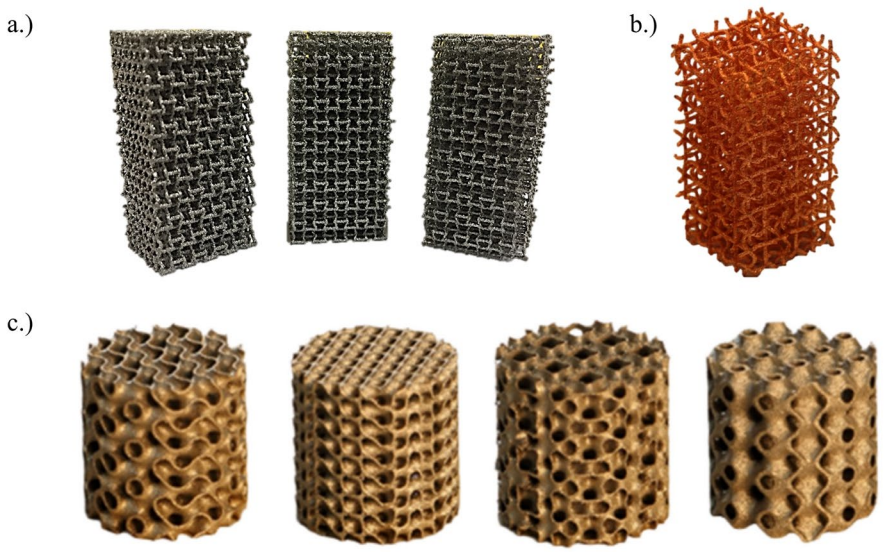

Fig. 4 Predesigned structures presented in this work: auxetic structures (**a**), auxetic chiral structures (**b**) and TPMS structures (**c**)

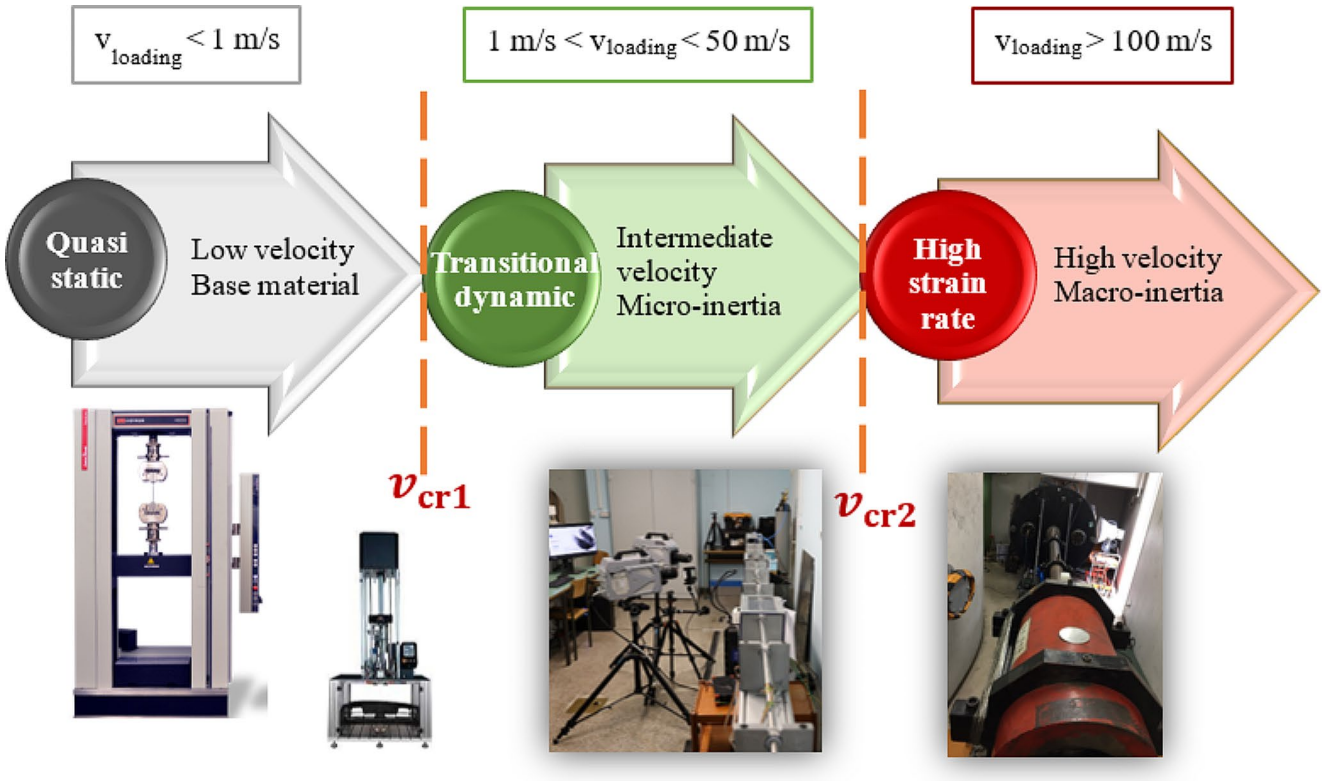

Fig. 5 Most commonly used testing methods for evaluation of the mechanical properties of cellular metamaterials

camera IR Flir SC 5000 (image frequency 608 Hz with a 0.02 K sensitive cooled mediumwave InSb detector).

When higher impact energies are needed at moderate impact velocities, drop tower devices can be employed to determine the mechanical and deformation behaviour of the metamaterials [55]. For dynamic compressive testing at higher strain rates above 1,000 s^{-1}, the Split Hopkinson Pressure Bar (SHPB) or its modified versions can be used. Most of the tests presented here were conducted using the Direct Impact Hopkinson Bar (DIHB) technique, specifically designed for the dynamic characterisation of cellular metamaterials [32, 33]. The DIHB setup, a modification of the classical Split Hopkinson Pressure Bar (SHPB) device with a 1500 mm bar length, enables the generation of higher strains in cellular materials. In this experimental configuration, the striker length of 350 mm is propelled within an accelerating barrel using pressurized gas, directly impacting the sample. This direct impact facilitates the direct transfer of kinetic energy from the striker to the specimen. However, the constrained space within the accelerating barrel and the deformation caused by the striker's passage pose a challenge for attaching measuring devices, such as strain gauges (the first one mounted on 300 mm and the other one 750 mm away from the samples), to the striker.

Consequently, direct attachment of strain gauges to the striker is not feasible. This limitation hinders our ability to measure the stress state at the striker-sample interface and observe and verify dynamic equilibrium. Therefore, the strain gauge data must be synchronised with high-speed camera images captured at 70,000 fps using a high-speed digital camera Photron FASTCAM SA Z and a 100 mm f/2.8 Macro USM lens. This combination provided accurate data for a comprehensive analysis of the material's deformation. The stress and strain values were obtained by processing and synchronising the strain gauge and camera measurements described in [56, 57].

A single-stage powder gun was employed for very high-strain rate (shock) compression tests. This device propels a projectile through the combustion gases generated by gunpowder detonation. Its successful application in determining aluminium foam's high strain rate behaviour [58] and auxetic structures [14] has been demonstrated. The powder gun comprises a high-strength breach, a barrel (diameter: 40 mm and length: 4000 mm), and a target chamber. For optical observation, windows, electrical measurements, and projectile cushioning were installed within the target chamber. The projectile sabot, constructed from polyethylene (UHMWPE), had a brass weight attached to its front to serve as a projectile driver. The cellular structure was secured to the brass weight using adhesive. Due to the target chamber being decompressed to a near vacuum using a vacuum pump, air resistance during testing was negligible.

While the single-stage powder gun can propel a projectile at velocities up to 1.5 km/s, the impact velocity was reduced to 220–250 m/s for the cellular metamaterials. This reduction ensured an engineering strain rate exceeding 10,000 1/s for all analysed cellular material samples.

The impact velocity and deformation behaviour of the cellular structures during impact were captured using the high-speed video camera HPV-1 (manufactured by SHIMADZU, image acquisition number: 100, maximum resolution: 1 µs). The impact pressure of the auxetic cellular structure on the rigid wall was measured with the PVDF measuring device (Piezo-Film Voltmeter, PVF2 11-, 125EK, Dynasen), as previously employed in Tanaka et al.'s experiments [58].

All experiments used an appropriate number of samples to obtain a statistically representative average response, never less than three for each load case.

Computational Modelling

Computational modelling offers an excellent tool for analyzing the behaviour of cellular metamaterials at different strain rates. With that method, the costs of experimental testing can be decreased, but it should be done using carefully validated models.

The first step towards successful simulation is the correct geometric representation of cellular metamaterial. The fabricated aluminium open-cell foam samples necessitate a sufficiently high-resolution CT scan to capture geometric details and allow for accurate metallic phase segmentation. During the early study of mesh refining, geometric convergence is guaranteed.

The auxetic strut-based cellular structures were modelled with the beam finite elements to preserve the computational time and reach the large deformations of the metamaterials. The shell finite elements were used to discretise the TPMS lattices. Using beam and shell finite elements allowed us to reduce the problem's computational complexity while maintaining a good accuracy level, neglecting the local variations in cross-sectional shape and size. The MSLattice code was used to generate the CAD geometry of the lattices, while PrePoMax software was used to mesh the TPMS lattices [59]. The final mesh can be seen in Fig. 6.

The boundary conditions were the same for all analysed metamaterials and defined in the LS-PrePost software, a powerful tool for defining complex loading conditions. The manufacturing imperfections resulting in plate thickness variation were indirectly considered using material parameters [50]. This was done by performing inverse parametric computational simulations, which use experimental data to determine the values of unknown parameters. The samples in FE simulations were placed between two plates, to which the following boundary conditions were prescribed: the bottom compression plate with all degrees of freedom fixed, the top compression plate with prescribed constant velocity towards the bottom plate (Fig. 6).

The elastoplastic material model (MAT_024) was used to describe the base material's constitutive behaviour of the analysed TPMS lattices [60]. This model is a rate-dependent, piecewise-linear elastic-plastic model [61]. It is commonly used for modelling the behaviour of metals and alloys and is suitable for simulating the large deformations and plastic yielding in lattices under impact loading. Inverse computational simulations of loaded samples were performed to retrieve the same macroscopic simulation results measured in experimental testing for all metamaterials and an entire range of strains up to densification. This means that the material parameters (Young's modulus, hardening and failure definition) used in the MAT_024 model were adjusted until the simulated stress-strain curves matched the experimental data.

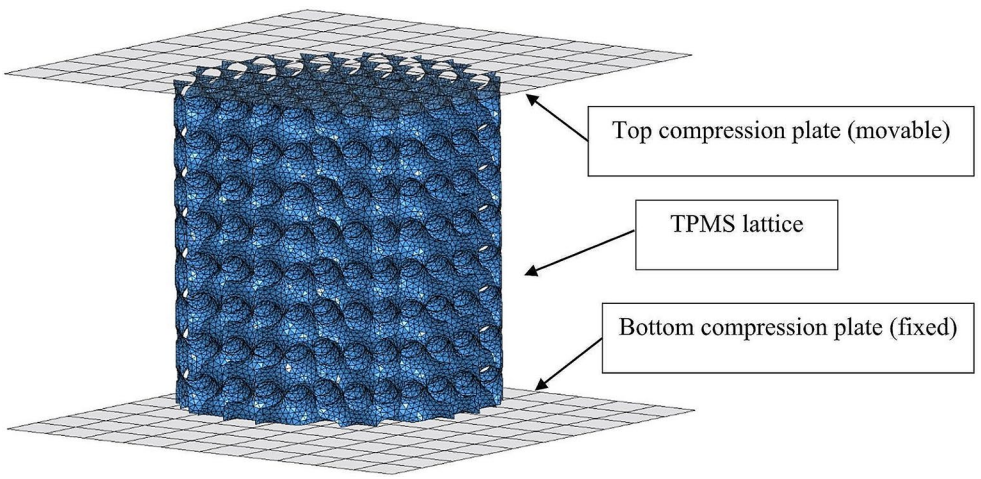

Fig. 6 Computational model of TPMS lattice

Results

Experimental Testing

The results of experimental testing of different cellular metamaterials are well documented in referenced literature in previous sections and are generally compared in this section. Several factors influence the attained Specific Energy Absorption (SEA), such as the base material type of structure, relative density, unit cell topology, and strain rate, making direct comparison challenging. Figure 7 compares the experimental findings of different structures under quasi-static compression loading regarding specific energy absorption (SEA) up to 50% strain. In Fig. 7, darker shading colours represent specimens with lower porosity in each analysed set of cellular structures, whereas lighter shading represents specimens with higher porosity.

It is clear that porosity and base material significantly impact SEA capacity. Low-porosity structures can absorb more mechanical energy through deformation than higher-porosity materials with lesser stiffness. A similar result may be drawn for base materials, with higher Young's modulus materials showing higher SEA capacity. In absolute terms, the best consistent SEA at 50% strain can be observed for TPMS, closed-cell foams and UniPore structures. It should be noted that in UniPore structures, densification already appears at 50% strain, and the shown SEA is thus the total SEA for this type of structure. Other analysed cellular structures densify at much higher strains, contributing to the total SEA capacity of these cellular structures. The TPMS structures generally outperform other structures at all analysed relative density levels. This is attributed to their sheet-based geometry, which enhances the mechanical properties compared to strut-based geometry in the case of auxetic and open-cell foams.

The relationship between porosity, base material, and SEA capacity can be further explored by examining the deformation mechanisms of different cellular structures. Closed-cell and TPMS foams, for instance, undergo a combination of elastic deformation, plastic deformation, and cell wall bending, allowing them to absorb significant energy before densification occurs. UniPore, open-cellular and analysed auxetic structures, on the other hand, rely primarily on tension-dominated elastic deformation, limiting their SEA capacity and making them more lightweight and compliant. The choice of cellular structure for a particular application will depend on the specific requirements of the application. If high SEA capacity is critical, TPMS, closed-cell foams or other structures with low porosity and high stiffness may be the best choice. However, if weight or compliance is more important, open-cell structures or other structures with higher porosity may be more suitable.

Materials' deformation behaviour at varying strain rates may be classified into homogeneous, transition, and shock modes [62]. In the homogeneous mode, inertia effects are insignificant, and deformation and collapse begin at the weakest region of the structure and are predominantly manifested as shear bands. At increasing loading velocities, inertia effects begin to dominate the response. Only limited transverse crushing of the structure at the impact

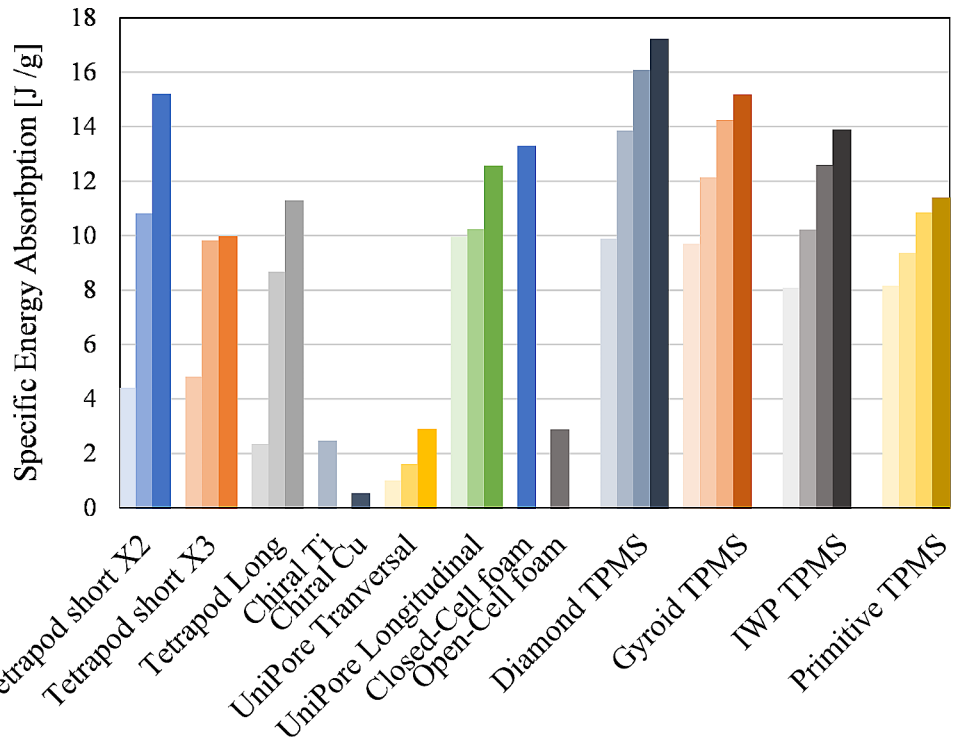

Fig. 7 Comparison of specific energy absorption capabilities of different cellular structures at quasi-static loading conditions [17]

deformation front is observed in shock mode, independent of the structure's weakest point position. The shock reaction is exhibited in a transition mode at lower strains, whereas the homogeneous mode arises at higher strains.

When considering the strain rate hardening effects in the cellular metamaterials, one of the most important indicators is critical velocity, where the deformation mode changes to shock mode, which results in enormous strain rate hardening [15] due to the inertia effects associated with the dynamic localisation of crushing at above critical strain rates [63]. Analyzing critical loading velocities at which the deformation mode changes is vital for using cellular metamaterials. Mainly, since they may be utilised as crash and shock absorbers in many contemporary composite constructions due to their distinctive deformation behaviour with the lengthy stress plateau zone, they can absorb a considerable quantity of mechanical energy. Numerous constitutive crushing models may be used to describe the dynamic deformation of cellular (porous) materials, as presented in [15]. The Rigid Power Law Hardening (R-PLH) model was used for this investigation because it provides high-accuracy estimates of shock-generated stress in the densification zone. The Rigid Power Law Hardening (R-PLH) model is a constitutive model used to describe the densification behaviour of cellular materials under dynamic loading conditions. It is based on the assumption that the material undergoes a power-law hardening with a constant strain rate sensitivity. The critical velocities for some selected cellular structures are provided in Fig. 8.

The comparison of critical velocities in Fig. 8 shows that, in general, the critical velocities increase with decreasing porosity, i.e., increased density of the metamaterial results in increased critical velocities.

The influence of the increased velocities on the deformation response in the experimental testing of selected TPMS metamaterials is shown in Fig. 9. The deformation response of IWP structures differs in QS and DIHB testing (Fig. 9). In the QS case, there is a localized failure in the middle of the sample, where the material has time to react and fails in the weakest layer with the most fabrication defects [26, 64]. The deformation is more uniformly distributed in the DIHB case, indicating the onset of micro-inertia influence at an increased deformation rate. This change in deformation mode due to inertia effects also influences the mechanical response and results in more significant strain rate hardening, as in the case of other structures. The deformation in the case of HSR loading is localized at the impacting side, which results in significant strain rate hardening (Fig. 10).

The mechanical responses of IWP TPMS structures at different loading velocities are shown in Fig. 10. The mechanical responses at lower strain rates are comparable, but the minor strain rate hardening is still visible. This results from micro inertia effects and the base material's strain rate hardening. The significant strain rate hardening is observed when the loading velocity is higher than the second critical velocity. The wavy plateau region results from the local crushing of each layer of unit cells of the metamaterial and is the most significant at HSR testing conditions.

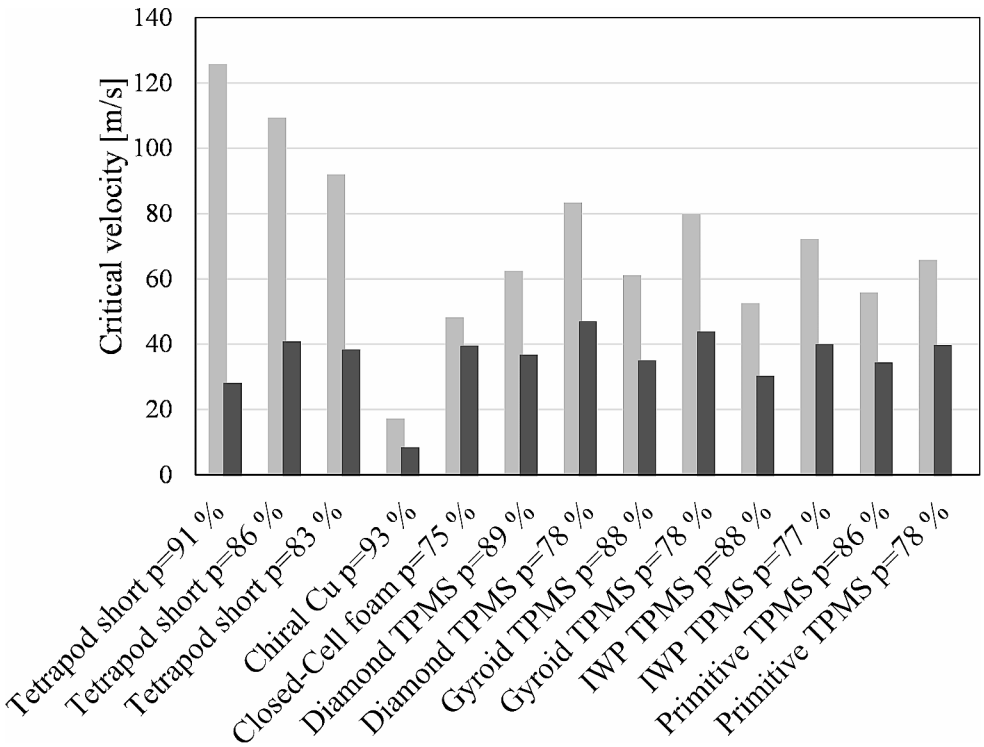

Fig. 8 Comparison of the first (black) and second (grey) critical velocities of different metamaterials with different porosities ("p" denotes the porosity of the samples)

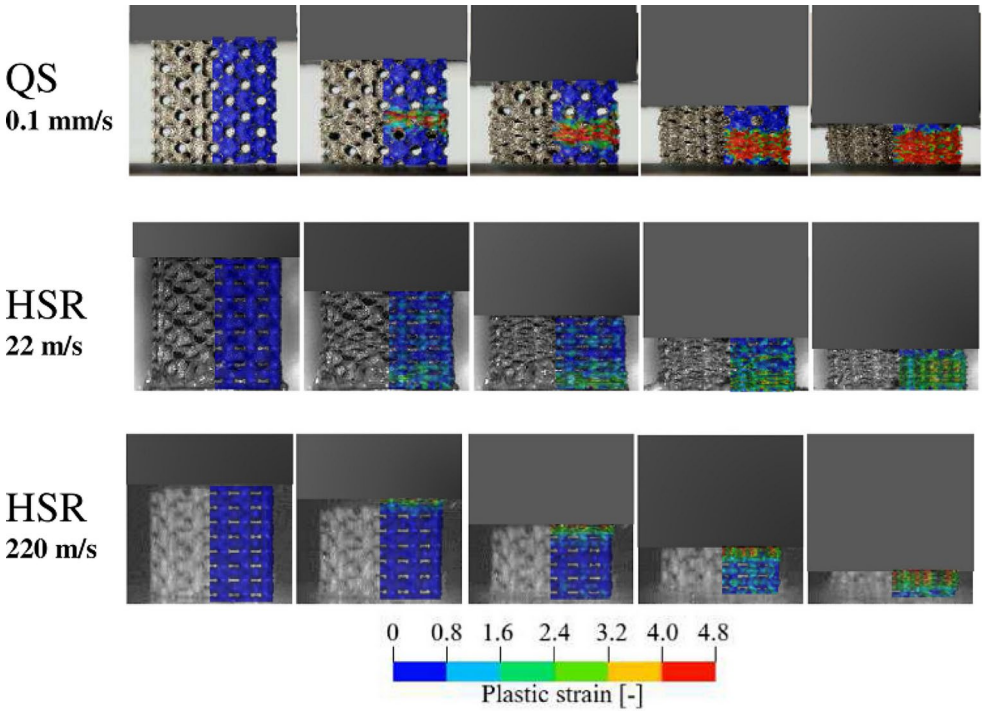

Fig. 9 Experimental and computational deformation behaviour of IWP TPMS structures at different loading velocities

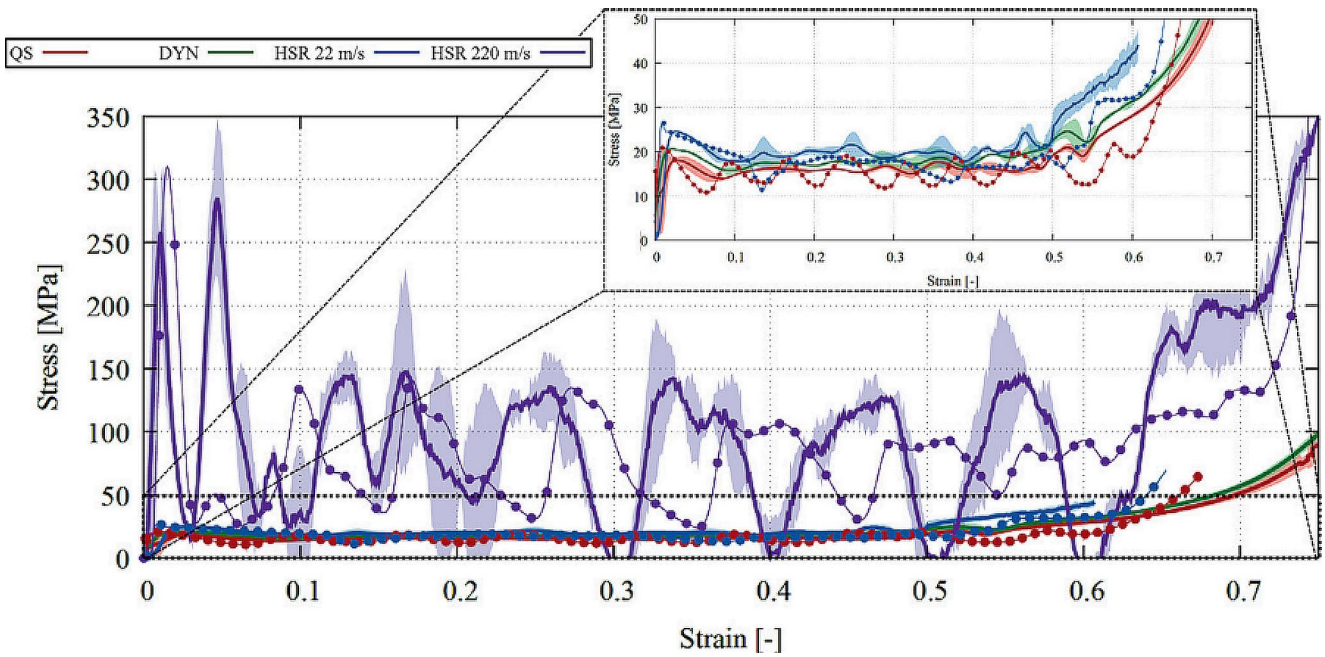

Fig. 10 Experimental (solid lines) and computational (solid line with dots) mechanical responses of IWP TPMS structures at different loading velocities

The evaluation of the strain rate hardening of different TPMS structures based on SEA comparison is shown in Fig. 11. The moderate strain rate hardening in the case of QS, DYN, and HSR at 22 m/s is observed, while the increase in SEA is significant in the case of testing above the second critical velocity at 220 m/s. The significant SEA increase is a consequence of the changed deformation mode, where most of the deformation happens on the impact front. The geometry and topology of the metamaterial don't govern the mechanical response anymore, and the density of the metamaterial takes a prominent role.

The SEA values of different cellular metamaterials at different loading velocities are further compared in Fig. 12, where the significant trade-off in SEA can be seen at strain

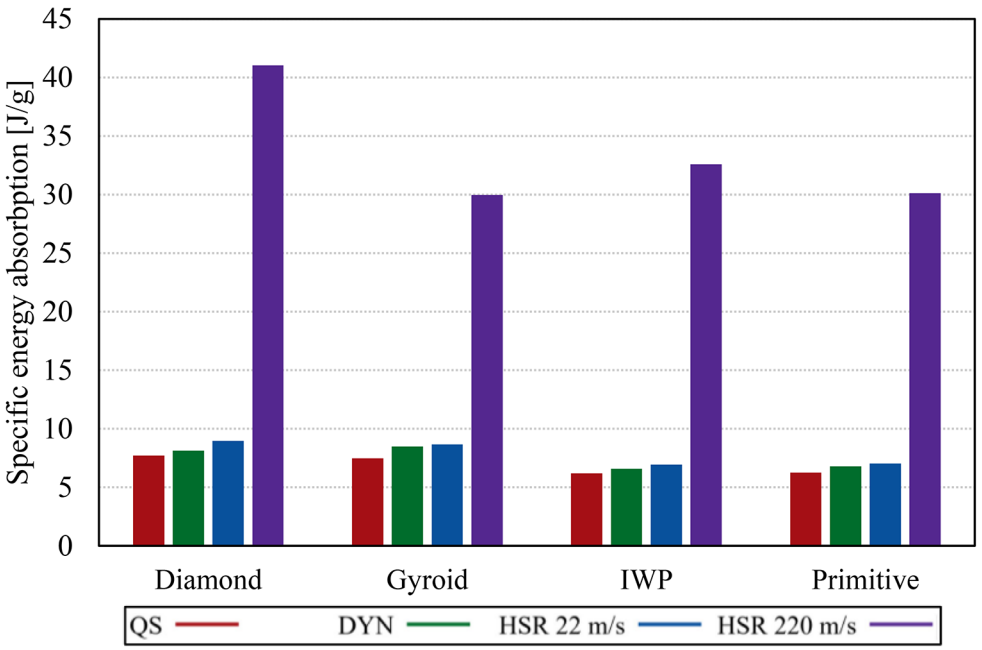

Fig. 11 The SEA values of different TPMS structures at different loading velocities

rates above 1000 1/s, where the shock deformation mode occurs for all analysed samples. The expensive and time-consuming high-strain rate experiments can be substituted with the validated computational models, which predict the mechanical responses at even higher strain rates that are experimentally analysed, as shown in Fig. 12.

Computational Simulations

The validation of computational models consists of a careful comparison of the deformation behaviour and mechanical response between the computational and experimental results. Furthermore, the validated computational models can also be used to study the use of these metamaterials in future applications. The computed mechanical response of selected Gyroid TPMS structure at different loading velocities is presented in Fig. 10. We can also precisely evaluate the critical velocities shown in Fig. 13 with carefully validated computational models.

The computational models also offer the possibility of predicting the behaviour of metamaterials at loading velocities and scenarios, which is not achievable in experimental testing, Fig. 12. The metamaterials can be used in blast protection as the core of the sandwich panels, where their topology can be determined and optimised using computational simulations [66]. The study was done for the auxetic structure [45] and the TPMS structures [66]. The typical deformation response is shown in Fig. 14, where the explosion causes the deformation of the bottom plate of the sandwich panel. This then proceeds to the core's deformation, which absorbs most of the impact energy with the deformation of the metamaterial. After the densification of the core, only the minority of the deformation is transferred to the top plate of the sandwich panel.

Besides blast loading, the sandwich panels filled with metamaterials can also be used for ballistic protection. The Fragment Simulating Projectile (FSP) loading was chosen for showcase, where the aluminium and titanium plates were tested first to determine the ballistic limit velocities [12]. The experimental tests and computational results of FSP impacting the titanium plate are shown in Fig. 15a. Good agreement can be observed, and this plate model was consequently used to simulate the impact of FSP on the sandwich panel (Fig. 15b). The geometry of the core that absorbs the energy of the localised impact can be optimised using these computational models for any expected loading scenario.

Conclusions

Strain rate hardening is a mechanical phenomenon observed in cellular metamaterials, where the material's stiffness increases with increasing strain rate. At elevated strain rates, the inertia of the individual cells or struts that constitute the cellular metamaterials becomes dominant. This behaviour is attributed to several factors, including micro inertia effects, strain rate hardening of base material, and mainly the inertia effects. Furthermore, as shown in this work, the geometry and topology of the metamaterials significantly influence the strain rate hardening. This causes a need for extensive mechanical characterisation of cellular metamaterials using experiments and computational simulations.

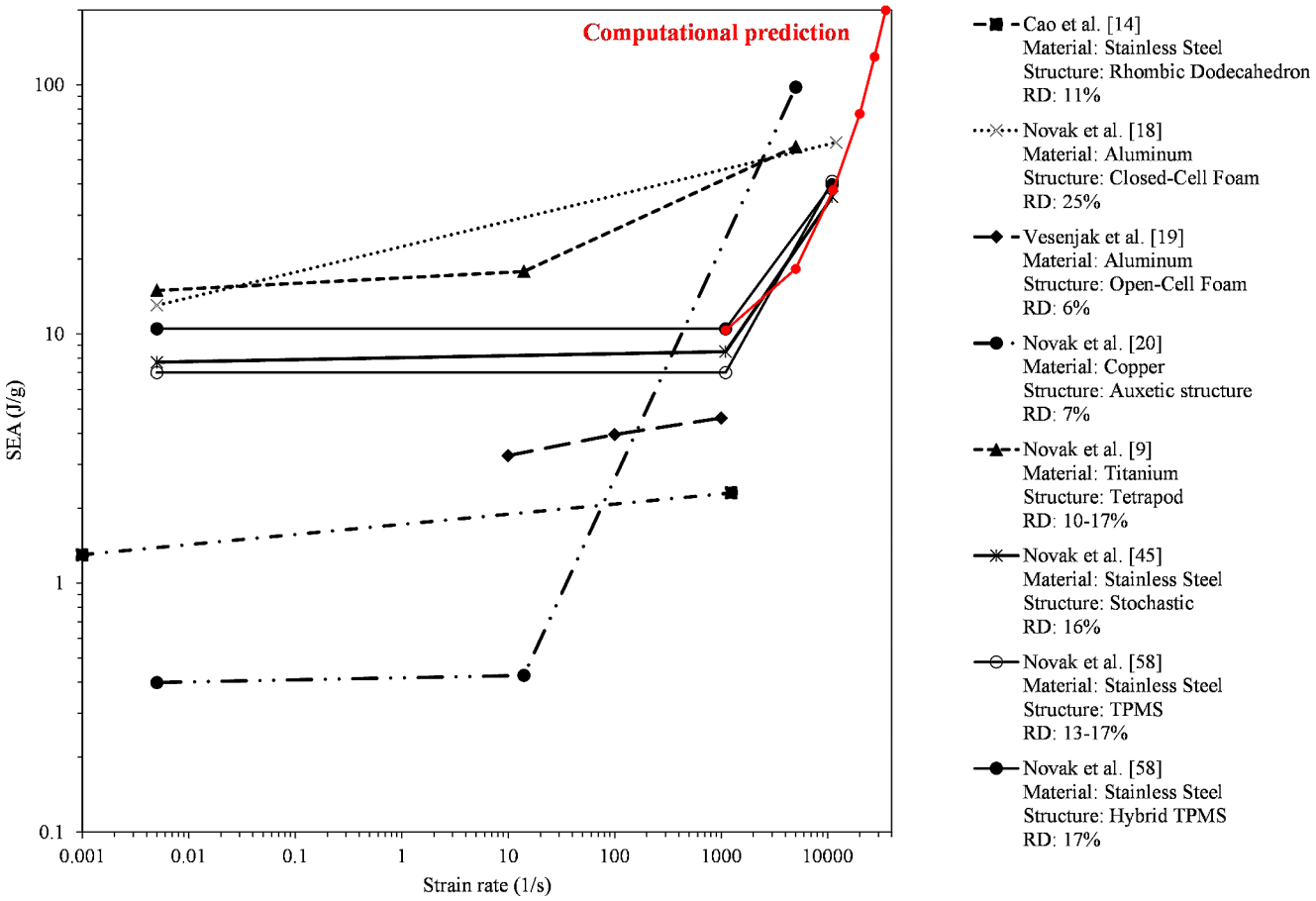

Fig. 12 SEA of different cellular structures tested at different strain rates (RD– Relative Density) [65]

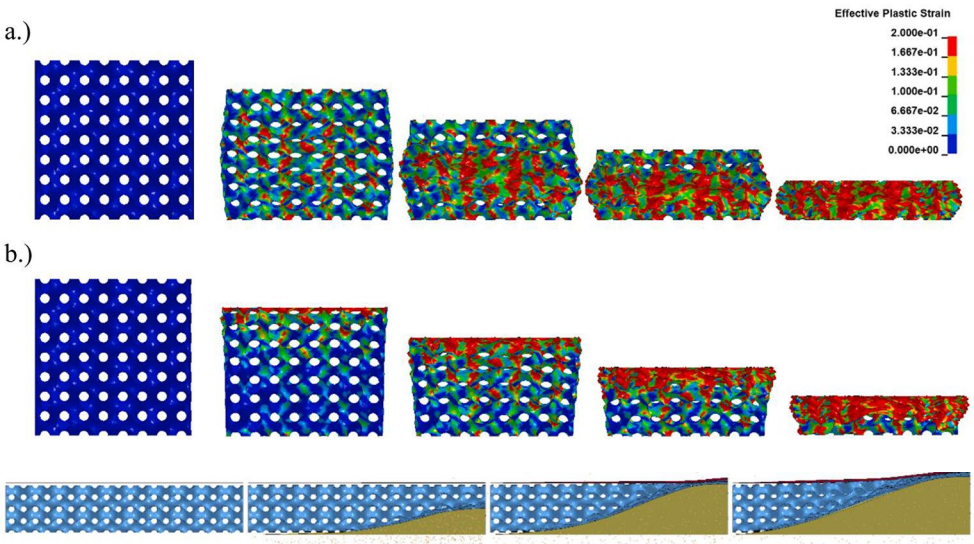

Fig. 13 The deformation behaviour of uniform Gyroid (21.9% RD) TPMS structure at loading velocity of (**a**) 30 m/s (homogeneous mode) and (**b**) 100 m/s (shock mode)– strain intervals: 16% [66]

Fig. 14 Deformation behaviour of TPMS-filled sandwich panel under blast loading [66]

A few different types of cellular metamaterials have been presented in this work, with a particular focus on their mechanical and deformation behaviour at different strain rates. The experimental results and validated computational models offer an excellent opportunity to study the behaviour of the metamaterials at different strain rates and explore the new applications where the metamaterials will be used in future. Understanding the multifaceted nature of strain rate hardening in cellular metamaterials requires extensive mechanical characterization using experiments

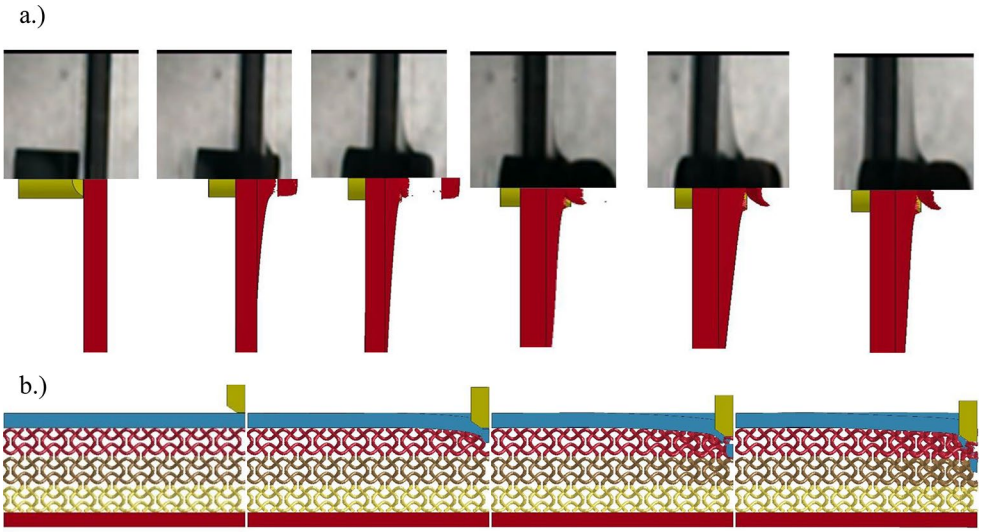

Fig. 15 Deformation behaviour of titanium plate (**a**) and sandwich panel (**b**) under FSP projectile impact [12]

and computational simulations. Experimental testing provides valuable insights into the mechanical behaviour of different metamaterials under various strain rates, while computational simulations offer a deeper understanding of the underlying mechanisms. The investigations show that, in general, the deformation mode change between quasi-static, intermediate and shock in metallic metamaterials depends on their porosity. The critical velocities separating the deformation modes decrease with increasing porosity, i.e., decreased density of the metamaterial results in reduced critical loading velocities. The shock deformation mode in cellular metamaterials is thus attainable at much lower loading velocities than in homogeneous (nonporous) materials.

The specific mechanisms of strain rate hardening in cellular metamaterials are still being investigated. Still, it is clear that inertia causes this phenomenon and significantly impacts the mechanical properties of these materials. Engineers can design cellular metamaterials with tailored mechanical behaviour for various applications by understanding and controlling strain rate hardening.

Acknowledgements The authors acknowledge the financial support from Slovenian Research (research core funding No. P2-0063).

Data Availability The raw/processed data required to reproduce these findings cannot be shared due to technical or time limitations.

Declarations

Conflict of Interest The authors have no competing interests to declare that are relevant to the content of this article.

References

1. Gibson LJ, Ashby MF (1997) Cellular solids: structure and properties. Cambridge University Press, Cambridge, U.K.
2. Banhart J (2013) Light-metal foams - history of innovation and technological challenges. Adv Eng Mater 15:82–111. https://doi.org/10.1002/adem.201200217
3. Banhart J (2001) Manufacture, characterization and application of cellular metals and metal foams. Prog Mater Sci 46:559–632
4. Duncan O, Shepherd T, Moroney C, Foster L, Venkatraman P, Winwood K, Allen T, Alderson A (2018) Review of Auxetic materials for sports Applications: Expanding options in Comfort and Protection. Appl Sci 8:941–974. https://doi.org/10.3390/app8060941
5. Jiang W, Ren X, Wang SL, Zhang XG, Zhang XY, Luo C, Xie YM, Scarpa F, Alderson A, Evans KE (2022) Manufacturing, characteristics and applications of auxetic foams: a state-of-the-art review. Compos Part B Eng 109733. https://doi.org/10.1016/j.compositesb.2022.109733
6. Novak N, Duncan O, Allen T, Alderson A, Vesenjak M, Ren Z (2021) Shear modulus of conventional and auxetic open-cell foam. Mech Mater 157:103818. https://doi.org/10.1016/j.mechmat.2021.103818
7. Winter RE, Cotton M, Harris EJ, Maw JR, Chapman DJ, Eakins DE, McShane G (2014) Plate-impact loading of cellular structures formed by selective laser melting. Model Simul Mater Sci Eng 22. https://doi.org/10.1088/0965-0393/22/2/025021
8. Zheng Z, Yu J, Wang C, Liao S, Liu Y (2013) Dynamic crushing of cellular materials: a unified framework of plastic shock wave models. Int J Impact Eng 53:29–43. https://doi.org/10.1016/j.ijimpeng.2012.06.012
9. Tancogne-Dejean T, Spierings AB, Mohr D (2016) Additively-manufactured metallic micro-lattice materials for high specific energy absorption under static and dynamic loading. Acta Mater 116:14–28. https://doi.org/10.1016/J.ACTAMAT.2016.05.054

10. Novak N, Vesenjak M, Ren Z (2017) Computational Simulation and optimization of functionally graded auxetic structures made from inverted tetrapods. Phys Status Solidi B 254. https://doi.org/10.1002/pssb.201600753
11. Novak N, Borovinšek M, Vesenjak M, Wormser M, Körner C, Tanaka S, Hokamoto K, Ren Z (2018) Crushing behavior of graded auxetic structures built from inverted tetrapods under Impact. Phys Status Solidi B 256:1–7. https://doi.org/10.1002/pssb.201800040
12. Novak N, Vesenjak M, Kennedy G, Thadhani N, Ren Z (2019) Response of Chiral Auxetic Composite Sandwich Panel to Fragment simulating Projectile Impact. Phys Status Solidi B 1900099:1–6. https://doi.org/10.1002/pssb.201900099
13. Fíla T, Zlámal P, Jiroušek O, Falta J, Koudelka P, Kytýř D, Doktor T, Valach J (2017) Impact testing of polymer-filled auxetics using Split Hopkinson pressure bar. Adv Eng Mater. n/a-n/a https://doi.org/10.1002/adem.201700076
14. Novak N, Hokamoto K, Vesenjak M, Ren Z (2018) Mechanical behaviour of auxetic cellular structures built from inverted tetrapods at high strain rates. Int J Impact Eng 122:83–90. https://doi.org/10.1016/j.ijimpeng.2018.08.001
15. Sun Y, Li QM (2018) Dynamic compressive behaviour of cellular materials: a review of phenomenon, mechanism and modelling. Int J Impact Eng 112:74–115. https://doi.org/10.1016/j.ijimpeng.2017.10.006
16. Zhang Y, Liu T, Ren H, Maskery I, Ashcroft I (2018) Dynamic compressive response of additively manufactured AlSi10Mg alloy hierarchical honeycomb structures. Compos Struct 195:45–59. https://doi.org/10.1016/J.COMPSTRUCT.2018.04.021
17. Novak N, Vesenjak M, Nishi M, Tanaka S, Hokamoto K, Ren Z (2021) Mechanical behavior of cellular materials—from quasi-static to high strain rate impact response, in: K. Hokamoto (Ed.), Explos. Shock. High-Strain Rate Phenom. Adv. Mater., Elsevier
18. AlMahri S, Santiago R, Lee D, Ramos H, Alabdouli H, Alteneiji M, Guan Z, Cantwell W, Alves M (2021) Evaluation of the dynamic response of triply periodic minimal surfaces subjected to high strain-rate compression. Addit Manuf 46:102220. https://doi.org/10.1016/j.addma.2021.102220
19. Ramos H, Santiago R, Soe S, Theobald P, Alves M (2022) Response of gyroid lattice structures to impact loads. Int J Impact Eng 164:104202. https://doi.org/10.1016/J.IJIMPENG.2022.104202
20. Cao X, Xiao D, Li Y, Wen W, Zhao T, Chen Z, Jiang Y, Fang D (2020) Dynamic compressive behavior of a modified additively manufactured rhombic dodecahedron 316L stainless steel lattice structure. Thin-Walled Struct 148:106586. https://doi.org/10.1016/j.tws.2019.106586
21. Harris JA, Winter RE, Mcshane GJ (2017) Impact response of additively manufactured metallic hybrid lattice materials. Int J Impact Eng 104:177–191. https://doi.org/10.1016/j.ijimpeng.2017.02.007
22. Sun Y, Li QM, Lowe T, McDonald SA, Withers PJ (2016) Investigation of strain-rate effect on the compressive behaviour of closed-cell aluminium foam by 3D image-based modelling. Mater Des 89:215–224. https://doi.org/10.1016/j.matdes.2015.09.109
23. Xi CQ, Li QM (2017) Meso-scale mechanism of compaction shock propagation in cellular materials. Int J Impact Eng 109:321–334. https://doi.org/10.1016/j.ijimpeng.2017.07.005
24. Novak N, Vesenjak M, Duarte I, Tanaka S, Hokamoto K, Krstulović-Opara L, Guo B, Chen P, Ren Z (2019) Compressive behaviour of closed-cell Aluminium Foam at different strain rates, materials (Basel). 12:4108. https://doi.org/10.3390/ma12244108
25. Vesenjak M, Veyhl C, Fiedler T (2012) Analysis of anisotropy and strain rate sensitivity of open-cell metal foam. Mater Sci Eng A 541:105–109. https://doi.org/10.1016/j.msea.2012.02.010
26. Novak N, Vesenjak M, Tanaka S, Hokamoto K, Ren Z (2020) Compressive behaviour of chiral auxetic cellular structures at different strain rates. Int J Impact Eng 141:103566. https://doi.org/10.1016/j.ijimpeng.2020.103566
27. Lehmhus D, Vesenjak M, de Schampheleire S, Fiedler T (2017) From stochastic foam to designed structure: balancing cost and performance of cellular metals. Mater (Basel) 10:1–32. https://doi.org/10.3390/ma10080922
28. Al-Ketan O, Rowshan R, Abu Al-Rub RKR (2018) Topology-mechanical property relationship of 3D printed strut, skeletal, and sheet based periodic metallic cellular materials. Addit Manuf 19:167–183. https://doi.org/10.1016/j.addma.2017.12.006
29. Borovinšek M, Vesenjak M, Jože M, Ren Z (2008) Computational Reconstruction of Scanned Aluminum Foams for virtual testing. J Serbian Soc Comput Mech 2:16–28
30. Duarte I, Vesenjak M, Krstulović-Opara L, Ren Z (2018) Crush performance of multifunctional hybrid foams based on an aluminium alloy open-cell foam skeleton. Polym Test 67:246–256. https://doi.org/10.1016/j.polymertesting.2018.03.009
31. Duarte I, Krstulović-Opara L, Dias-de-oliveira J, Vesenjak M (2019) Axial crush performance of polymer-aluminium alloy hybrid foam filled tubes. Thin-Walled Struct 138:124–136. https://doi.org/10.1016/j.tws.2019.01.040
32. Duarte I, Vesenjak M, Vide M (2019) J., Automated Continuous Production Line of Parts, Metals (Basel). 9 1–13
33. Gibson LJ, Ashby MF (1999) Cellular solids: structure and properties. Cambridge University Press
34. Vesenjak M, Borovinšek M, Fiedler T, Higa Y, Ren Z (2013) Structural characterisation of advanced pore morphology (APM) foam elements. Mater Lett 110:201–203. https://doi.org/10.1016/j.matlet.2013.08.026
35. Duarte I, Vesenjak M, Krstulović-Opara L (2016) Compressive behaviour of unconstrained and constrained integral-skin closed-cell aluminium foam. Compos Struct 154:231–238. https://doi.org/10.1016/j.compstruct.2016.07.038
36. Duarte I, Vesenjak M, Krstulović-Opara L, Ren Z (2015) Static and dynamic axial crush performance of in-situ foam-filled tubes. Compos Struct 124:128–139. https://doi.org/10.1016/j.compstruct.2015.01.014
37. Kovačič A, Novak N, Vesenjak M, Dobnik Dubrovski P, Ren Z (2018) Geometrical and mechanical properties of polyamide PA 12 bonds in composite advanced pore morphology (APM) foam structures. Arch Civ Mech Eng 18:1198–1206. https://doi.org/10.1016/j.acme.2018.01.004
38. Ulbin M, Borovinšek M, Higa Y, Shimojima K, Vesenjak M, Ren Z (2014) Internal structure characterization of AlSi7 and AlSi10 advanced pore morphology (APM) foam elements. Mater Lett 136:416–419. https://doi.org/10.1016/j.matlet.2014.08.056
39. Ulbin M, Vesenjak M, Borovinšek M, Duarte I, Higa Y, Shimojima K, Ren Z (2018) Detailed Analysis of Closed-Cell Aluminum Alloy Foam Internal Structure Changes during compressive deformation. Adv Eng Mater 20:1–8. https://doi.org/10.1002/adem.201800164
40. Duarte I, Vesenjak M, Krstulović-Opara L, Ren Z (2015) Compressive performance evaluation of APM (Advanced Pore morphology) foam filled tubes. Compos Struct 134:409–420. https://doi.org/10.1016/j.compstruct.2015.08.097
41. Vesenjak M, Duarte I, Baumeister J, Göhler H, Krstulović-Opara L, Ren Z (2020) Bending performance evaluation of aluminium alloy tubes filled with different cellular metal cores. Compos Struct 234:111748. https://doi.org/10.1016/j.compstruct.2019.111748
42. Novak N, Vesenjak M, Ren Z (2016) Auxetic cellular materials - a review, Strojniški Vestn. - J Mech Eng 62:485–493. https://doi.org/10.5545/sv-jme.2016.3656
43. Feng J, Fu J, Yao X, He Y (2022) Triply periodic minimal surface (TPMS) porous structures: from multi-scale design, precise additive manufacturing to multidisciplinary applications. Int J Extrem Manuf 4:022001. https://doi.org/10.1088/2631-7990/ac5be6

44. Schwerdtfeger J, Heinl P, Singer RF, Körner C (2010) Auxetic cellular structures through selective electron beam melting. Phys Status Solidi B 247:269–272. https://doi.org/10.1002/pssb.200945513
45. Novak N, Starčevič L, Vesenjak M, Ren Z (2019) Blast response study of the sandwich composite panels with 3D chiral auxetic core. Compos Struct 210:167–178. https://doi.org/10.1016/j.compstruct.2018.11.050
46. Körner C, Liebold-Ribeiro Y (2014) A systematic approach to identify cellular auxetic materials. Smart Mater Struct 24:025013. https://doi.org/10.1088/0964-1726/24/2/025013
47. Novak N, Krstulović L, Ren Z, Vesenjak M (2020) Mechanical properties of hybrid metamaterial with auxetic chiral cellular structure and silicon filler. Compos Struct 234. https://doi.org/10.1016/j.compstruct.2019.111718
48. Kapfer SC, Hyde ST, Mecke K, Arns CH (2011) Schröder-Turk, minimal surface scaffold designs for tissue engineering. Biomaterials. https://doi.org/10.1016/j.biomaterials.2011.06.012
49. Torquato S, Donev A (2004) Minimal surfaces and multifunctionality. Proc R Soc Math Phys Eng Sci 460:1849–1856. https://doi.org/10.1098/rspa.2003.1269
50. Novak N, Al-Ketan O, Krstulović-Opara L, Rowshan R, Al-rub RKA, Vesenjak M, Ren Z, Abu Al-Rub RK, Vesenjak M, Ren Z (2021) Quasi-static and dynamic compressive behaviour of sheet TPMS cellular. Compos Struct 266:113801. https://doi.org/10.1016/j.compstruct.2021.113801
51. Novak N, Al-Ketan O, Mauko A, Yilmaz YE, Krstulović-Opara L, Tanaka S, Hokamoto K, Rowshan R, Al-Rub RA, Vesenjak M, Ren Z (2023) Impact loading of additively manufactured metallic stochastic sheet-based cellular material. Int J Impact Eng 174:104527. https://doi.org/10.1016/j.ijimpeng.2023.104527
52. ISO 13314:2011 - Mechanical testing of metals - ductility testing - compression test for porous and cellular metals, International Organization for Standardization, Geneva, Switzerland (2011) www.iso.org
53. Krstulović-Opara L, Surjak M, Vesenjak M, Tonković Z, Kodvanj J, Domazet Ž (2015) Comparison of infrared and 3D digital image correlation techniques applied for mechanical testing of materials. Infrared Phys Technol 73:166–174. https://doi.org/10.1016/j.infrared.2015.09.014
54. Krstulović-Opara L, Vesenjak M, Duarte I, Ren Z (2016) Infrared thermography as a method for energy absorption evaluation of metal foams. Mater Today Proc 3:1025–1030. https://doi.org/10.1016/j.matpr.2016.03.041
55. Novak N, Al-Rifaie H, Airoldi A, Krstulović-Opara L, Łodygowski T, Ren Z, Vesenjak M (2023) Quasi-static and impact behaviour of foam-filled graded auxetic panel. Int J Impact Eng 178:104606. https://doi.org/10.1016/j.ijimpeng.2023.104606
56. Yu L, Pan B (2017) Color Stereo-Digital image correlation method using a single 3CCD Color Camera. Exp Mech 57:649–657. https://doi.org/10.1007/s11340-017-0253-7
57. Liu J, He S, Zhao H, Li G, Wang M (2018) Experimental investigation on the dynamic behaviour of metal foam: from yield to densification. Int J Impact Eng 114:69–77. https://doi.org/10.1016/j.ijimpeng.2017.12.016
58. Tanaka S, Hokamoto K, Irie S, Okano T, Ren Z, Vesenjak M, Itoh S (2011) High-velocity impact experiment of aluminum foam sample using powder gun. Meas J Int Meas Confed 44:2185–2189. https://doi.org/10.1016/j.measurement.2011.07.018
59. Borovinšek M, PrePoMax (n.d.). https://prepomax.fs.um.si/
60. Hallquist J (2007) LS-DYNA keyword user's manual, Livermore Software Technology Corporation, Livermore, California
61. Marzi S, Hesebeck O, Brede M, Kleiner F, Rate-Dependent A (2009) Elasto-Plastic Cohesive Zone mixed-Mode Model for Crash Analysis of Adhesively Bonded joints, in: 7th Eur. LS-DYNA Conf
62. Zheng Z, Yu J, Li J (2005) Dynamic crushing of 2D cellular structures: a finite element study. Int J Impact Eng 32:650–664. https://doi.org/10.1016/j.ijimpeng.2005.05.007
63. Tan PJ, Reid SR, Harrigan JJ, Zou Z, Li S (2005) Dynamic compressive strength properties of aluminium foams. Part I - experimental data and observations. J Mech Phys Solids 53:2174–2205. https://doi.org/10.1016/j.jmps.2005.05.007
64. Novak N, Vesenjak M, Krstulović-Opara L, Ren Z (2018) Mechanical characterisation of auxetic cellular structures built from inverted tetrapods. Compos Struct 196:96–107. https://doi.org/10.1016/j.compstruct.2018.05.024
65. Novak N, Tanaka S, Hokamoto K, Mauko A, Emre Y (2023) High strain rate mechanical behaviour of uniform and hybrid metallic TPMS cellular structures. Thin-Walled Struct 191:111109. https://doi.org/10.1016/j.tws.2023.111109
66. Novak N, Borovinšek M, Al-ketan O, Ren Z, Vesenjak M (2022) Impact and blast resistance of uniform and graded sandwich panels with TPMS cellular structures. Compos Struct 300. https://doi.org/10.1016/j.compstruct.2022.116174